Propagation of bioluminescent signals to near-surface from mesopelagic waters

Tonizzo, Alberto, Russell, Brandon, Sullivan, James, Twardowski, Michael

Alberto Tonizzo, Brandon J. Russell, James M. Sullivan, Michael S. Twardowski, "Propagation of bioluminescent signals to near-surface from mesopelagic waters," Proc. SPIE 10631, Ocean Sensing and Monitoring X, 1063113 (25 May 2018); doi: 10.1117/12.2310006

SPIE.

Event: SPIE Defense + Security, 2018, Orlando, Florida, United States

Propagation of bioluminescent signals to near-surface from mesopelagic waters

Alberto Tonizzo*[a], Brandon J. Russell[b], James M. Sullivan[b], and Michael S. Twardowski[b]
[a]AWF Consulting, Inc. 1166 6th Ave, Vero Beach, FL 32960 (United States); [b]Harbor Branch Oceanographic Institute 5600 N US Highway 1, Fort Pierce, FL 34946 (United States)
*alberto.tonizzo@gmail.com

ABSTRACT

Bioluminescence is a striking and ubiquitous source of light in the global ocean, utilized in a variety of ecologically important communication, camouflage, and predator deterrence functions. It can be prevalent in surface waters at night and at most times in mesopelagic waters (≈200-1000m) where ambient light approaches a weak, asymptotic radiance field. The propagation of bioluminescent signals, and therefore the distance at which these signals can be detected, is dependent upon the inherent optical properties (IOPs) of the water column. The effects of IOPs on the propagation of light from isotropic point sources embedded in bioluminescent layers were examined in terms of emitted signal against background radiance throughout the water column, i.e., a metric defining the required ability to detect the emissions.

Keywords: Bioluminescence, radiative transfer, radiometry, ocean optics.

1. INTRODUCTION

Bioluminescence (BL) is the emission of visible light by living organisms, typically as a result of proximal small scale shear. BL can be found in most marine habitats, both pelagic and benthic, and at all depths. However, it is most commonly found in surface to mesopelagic depths [1]. The reasons for the wide distribution of BL within marine organisms are various and include strategies for predator avoidance, prey location and attraction. There are many physiologically different systems of BL [2]. Due to the diverse physiologies, the bioluminescent emissions of different organisms can spectrally vary. The majority of pelagic and deep sea organisms emit light with a wavelength between 450 and 490 nm, corresponding to blue light which has optimal transmission through oceanic water [3]. Coastal and some bottom living organisms emit a greener light with emission wavelengths between 490 and 520 nm [4-5]. The interest in organisms producing light upon mechanical stimulation is not only to understand the organism-specific BL potential and ecological advantage; light production as a function of mechanical stimulation provides a direct visual method of identifying surface and subsurface objects. On the other hand BL is relevant in the development of strategies to reduce the risk of detection. The objective of this study is to use radiative transfer simulations to analyze the behavior of bioluminescent signal for different inherent optical properties (IOPs) and depths of the bioluminescent layer ranging from near-surface to mesopelagic depths. BL is an attractive candidate for multi- or hyper-spectral analysis: ideal bands can be selected depending on the IOPs of the water and the spectral shape of the bioluminescent signal, so one could have one "signal" band in which BL is detected and multiple "background" bands related to noise.

2. RADIATIVE TRANSFER COMPUTATIONS

Hydrolight 5 radiative transfer software (Sequoia Scientific, Inc.) can model a horizontally homogeneous layer of BL if the BL spectral source function (S_0) is known. $S_0(z,\lambda)$ (in units of W m^{-3} nm^{-1}) can be idealized as a hyperbolic tangent function with depth and a Gaussian function in wavelength [6]. Mobley [6] estimated an integrated value of ~10^{-5} W m^{-3} for typical concentrations of dinoflagellates, emitting ~10^{10} photons s^{-1} with an average wavelength of 480nm. However Lapota [7] observed values of ~10^{14} photons s^{-1} during periods of high BL in the Arabian Sea, therefore we assume total (i.e. integrated over wavelength) S_0 to be 0.001 W m^{-3} in our simulations, since we are interested in the effects of high values of BL for this preliminary assessment (but not extreme). It has to be noted that individual organisms act like point sources, when mechanically-stimulated BL is emitted, therefore the simulated scenario corresponds to the case of an extended layer of point source emitting organisms, e.g., which may be encountered when experiencing large scale shear from a large object moving through the water. Instead of a Gaussian curve as a function of the wavelength, we use the spectral shape reported in Moline et al. [8], corresponding to phytoplankton and copepods isolated and measured in

Ocean Sensing and Monitoring X, edited by Weilin (Will) Hou, Robert A. Arnone, Proc. of SPIE
Vol. 10631, 1063113 · © 2018 SPIE · CCC code: 0277-786X/18/$18 · doi: 10.1117/12.2310006

laboratory and based on observed natural abundances and patters. $S_0(z,\lambda)$ is normalized by setting its spectral integral, i.e. $\int_{350nm}^{650nm} S_0(\lambda)d\lambda$, equal to 0.001 W m^{-3}.

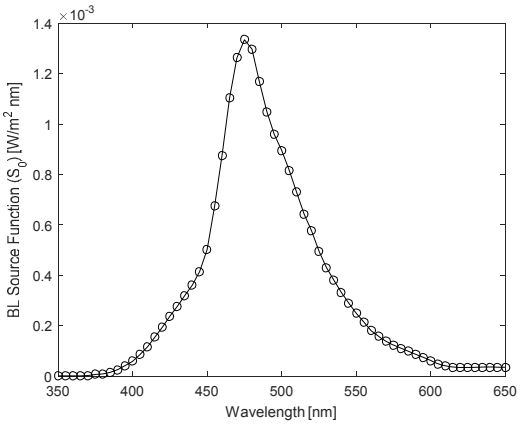

Figure 1. Spectral S_0 from Moline et al. [8] (normalized to 0.001 W m^{-3}). Sampling wavelengths are taken at 5 nm resolution.

2.1 Example station: BIOSOPE campaign

As a representative station to illustrate the propagation of BL from deep waters to surface, we select a station ("Station 4") recorded during the BIOSOPE campaign in the Southeast Pacific Ocean, in very clear oceanic (Case 1) waters [9]. Absorption and attenuation of particulate and dissolved matter (a_{pg} and c_{pg}, respectively) were measured by a WET Labs ac9 instrument at 412, 443, 490, 510, 555, 630, 650, 676, 715 nm; backscattering of particulate matter (b_{bp}) was measured by a WET Labs ECO BB3 at 462, 532, 657 nm, the particulate scattering phase function is parameterized in function of the particulate backscattering ratio $B_p = b_{bp}/b_p$. Figure 2 shows the vertical profiles of the total attenuation coefficient (including water). Raman scattering was included in the simulations but chlorophyll fluorescence was not, it being outside of the range of wavelengths of interest (i.e. 676nm). Default atmospheric parameters were used for all runs, with the user-defined sky irradiance equal to the spectral irradiance of the moon (whose zenith angle is set at 30°) reported by Cramer et al. [10], to simulate nighttime conditions (Figure 3). The cloud cover was kept at 0%; cloudy conditions were also simulated but had negligible effects on the results, as previously reported by Rohr et al. [11].

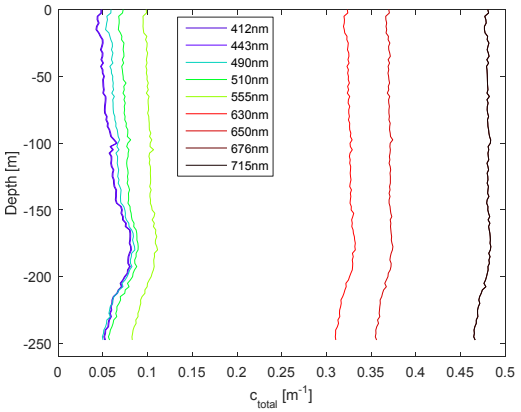

Figure 2. Vertical profiles of the beam attenuation coefficient at the ac9 wavelengths for the sample station recorded during BIOSOPE.

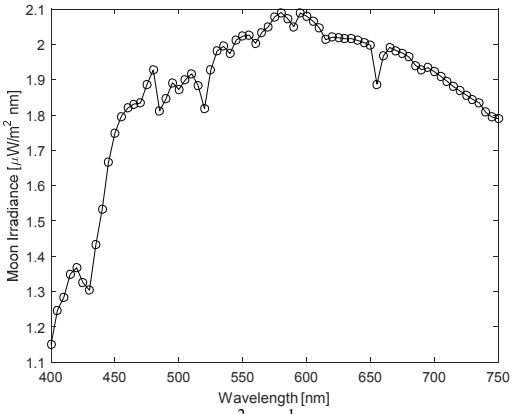

Figure 3. Spectral irradiance of the Moon in units of μW m^{-2} nm^{-1} taken from Cramer et. al [10].

For simplicity, a BL layer is modeled as a uniform layer, 10 m thick, moving from just below the surface of the ocean to mesopelagic depths (at 2.5 m resolution), where source were reported to be found, for instance, by Widder et al. [12] in the Gulf of Maine. Figure 4 shows an example from one model simulation, with the "stimulation" of BL occurring between 245 and 255 m depth. In such clear waters, the BL signal propagates far through the water column and the depth-dependent upwelling radiance, L_u is strongly affected by the presence of the bioluminescent layer.

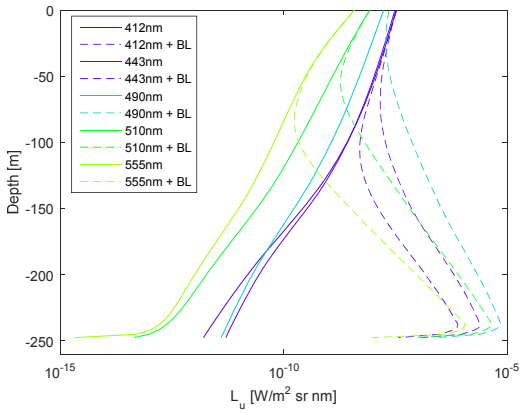

Figure 4. Vertical profile of upwelling radiance, L_u with ("+ BL") and without a bioluminescent layer located between 245 and 255 m depth. Only blue-green wavelengths are shown because BL signal outside this wavelength range is negligible.

If we assume that the background radiance is the upwelling radiance at the surface without the presence of any BL (L_u), then the ratio of propagated emission signal to the background radiance, which from the perspective of a detection system is also the signal to noise ratio (SNR), for a quantum noise limited system is given by Rohr et al. [11]:

$$SNR = 20\log_{10}\left[\left(L_{u,BL} - L_u\right)/L_u^{1/2}\right] \quad (1)$$

Where $L_{u,BL}$ is the upwelling radiance in the presence of a bioluminescent layer at a varied depth. Results of calculations are summarized in Figure 5 where the SNR for a Satlantic HyperOCR, a commercially available hyperspectral radiance sensor, is also shown. The maximum depth at which BL can be detected is given by the intersect of the sensor's SNR and the system's (any curve section to the right of the 10dB detection limit could be theoretically detected) and for the example station it is remarkably ~160 m at 490 nm. We note that the SNR is spectrally dependent, as noted by Moline et al. [8]. Therefore the spectral shape of the upwelling radiance may have the potential to be used for estimating the depth of the bioluminescent layer [13].

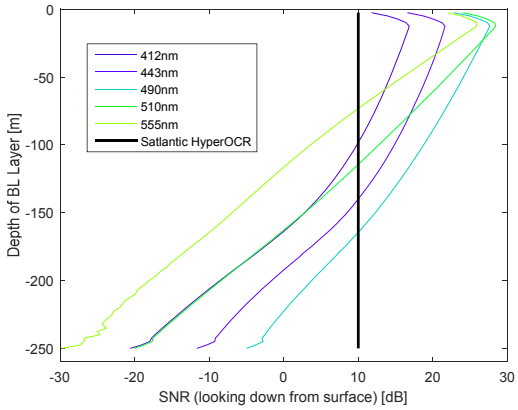

Figure 5. Ratio of BL signal to background radiance "noise" at night observed at the surface when the depth of the BL layer is varied throughout the water column. IOPs for this sample station were recorded in very clear water from the South Pacific gyre during the BIOSOPE field campaign. The vertical black line is the SNR for a Satlantic HyperOCR radiance sensor. Results show, for these waters, a BL layer at 160 m would be resolvable at the surface at 490 nm with this sensor.

2.2 BL database

Considering the same assumptions for the bioluminescent layer as before, we created a synthetic dataset representative of the coastal and open ocean with varying depths of the layer and with varying IOPs, related to chlorophyll concentration, [Chl], in units of mg m^{-3}. The BL layer was modeled as a uniform layer, 10 m thick, moving from 200 to 10 m depth. To save computational time and for a qualitative understanding of the physics, the simulated stimulation of bioluminescent organisms occurs every 10 m and the output wavelengths for radiances were selected to be 412, 443, 490, 510 and 555 nm only. The total absorption coefficient (a_{tot}) is given by the sum of water (a_w), phytoplankton (a_{phy}), non-algal particles (a_{NAP}) and colored dissolved organic matter (a_{CDOM}) absorption, i.e.:

$$a_{tot}(\lambda) = a_w(\lambda) + a_{phy}(\lambda) + a_{NAP}(\lambda) + a_{CDOM}(\lambda). \quad (2)$$

a_w is taken from Pope and Fry [14]. a_{phy} is calculated from [Chl] and from spectrally averaged absorption coefficients of micro- and pico-plankton ($\bar{a}_{micro}(\lambda)$ and $\bar{a}_{pico}(\lambda)$, respectively) [15]:

$$a_{phy}(\lambda) = [Chl] * \left(\left[S_f * \bar{a}_{pico}(\lambda)\right] + \left[\left(1 - S_f\right) * \bar{a}_{micro}(\lambda)\right]\right). \quad (3)$$

S_f = [0.25, 0.75] is the shape factor and [Chl] assumes 5 values, logarithmically spaced between 0.01 and 10 mg m^{-3}. a_{NAP} is given by [16]:

$$a_{NAP}(\lambda) = a_{NAP}(440) * e^{-0.011(\lambda - 440)}, \quad (4)$$

where $a_{NAP}(440)$, the absorption coefficient of non-algal particles at 440 nm, is equal to R_{NAP}* $a_{phy}(440)$, with R_{NAP} = [0.1, 1]. Similarly we use an exponentially decaying expression for the absorption of CDOM [17]:

$$a_{CDOM}(\lambda) = a_{CDOM}(440) * e^{-0.014(\lambda - 440)}, \quad (5)$$

where $a_{CDOM}(440)$, the absorption coefficient of colored dissolved organic matter at 440 nm, is equal to R_{CDOM}* $a_{phy}(440)$, with R_{CDOM} = [0.1, 1]. We note the parameters in the bio-optical model cover a limited subset of the naturally occurring variability of oceanic waters but bracket the range of possibilities suitable to understand the observed phenomena. The particulate scattering b_p is calculated at 550 nm from [18]:

$$b_p(550) = 0.416[Chl]^{0.766}. \quad (6)$$

It is extrapolated to other wavelengths according to [19]:

$$b_p(\lambda) = b_p(550) * \left(\frac{\lambda}{550}\right)^{v([Chl])}, \quad (7)$$

where $v([Chl]) = 0.5(\text{Log}[Chl] - 0.3)$ when $0.01 \leq [Chl] \leq 2$ mg m^{-3} and $v([Chl]) = 0$ when $[Chl] > 2$ mg m^{-3}. IOPs inputs for Hydrolight are the particulate and dissolved absorption coefficient, $a_{pg} = a_{phy} + a_{NAP} + a_{CDOM}$, the particulate and dissolved attenuation coefficient, $c_{pg} = a_{pg} + b_p$ and the particulate backscattering coefficient, b_{bp} calculated from [20] as:

$$b_{bp} = b_p \tilde{b}_{bp} = b_p * 0.0096[Chl]^{-0.253}, \quad (8)$$

where $\tilde{b}_{bp}$ or B_p is the particulate backscattering ratio. As for the example station recorded during BIOSOPE, Raman scattering was included in the simulations but chlorophyll fluorescence was not. Default atmospheric parameters were used for all runs, with the user-defined sky irradiance equal to the spectral irradiance of the moon (whose zenith angle is set at 30°) reported by Cramer et al. [10], to simulate nighttime conditions (Figure 3). The cloud cover was kept constant at 0%.

The plots in Figure 6 show the effect of increasing depth of the bioluminescent layer for a set of moderately turbid, Case 2 conditions (all related to the same [Chl] ~1.8 mg m^{-3}). The different curves of upwelling radiances correspond to different optical depths (i.e. $\tau^{490} = \int c_{tot}^{490}(z)dz = c_{tot}^{490} z$, in homogeneous waters), which are related to the varying concentrations of NAP and CDOM (linked to R_{NAP} and R_{CDOM}, respectively). The intensity of the upwelling radiance is highest at 490 nm when the bioluminescent layer is at 10 m depth but the maximum progressively red-shifts toward 510 nm as the layer is stimulated at greater depths. The behavior of the radiance spectrum is similar to that reported by Moline et al. [8], as they were also studying a selected site near the coast of New Jersey, characterized by mostly Case 2 waters. Higher transmission of light at 510 nm with respect to 490 nm is consistent with the total absorption spectrum of Case 2 waters shown in the left panel of Figure 7. In Case 1 waters ([Chl] ~0.06 mg m^{-3}), the total absorption coefficient is larger at 490 nm than it is at 443 nm, as shown in the right panel of Figure 7. Consequently, for very clear water, when light passes through a larger volume of water (as BL is stimulated deeper in the water column), it is absorbed preferentially at 490 nm and upwelling radiances become highest at 443 nm, i.e., there is now a blue-shift (Figure 8).

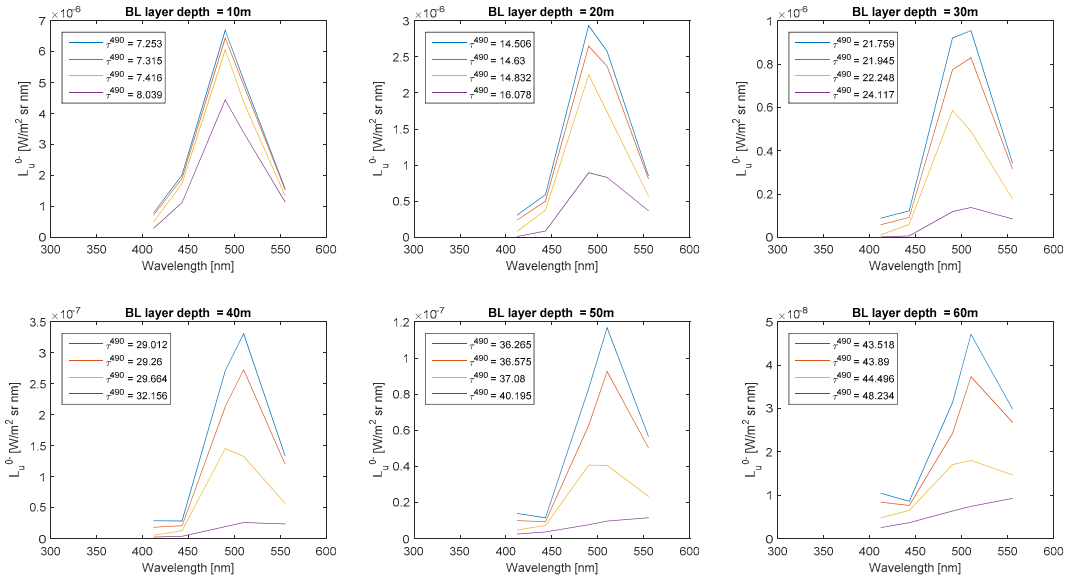

Figure 6. Upwelling radiance at surface for depths of a bioluminescent layer down to 60 m for Case 2 waters with [Chl] ~1.8 mg m^{-3}. The different curves of upwelling radiances correspond to different optical depths (τ^{490}), which are related to the varying concentrations of NAP and CDOM (linked to R_{NAP} and R_{CDOM}, respectively; see Figure 7). The intensity of the upwelling radiance is highest at 490 nm when the bioluminescent layer is at 10 m depth but the maximum progressively red-shifts toward 510 nm as the layer is stimulated at greater depths.

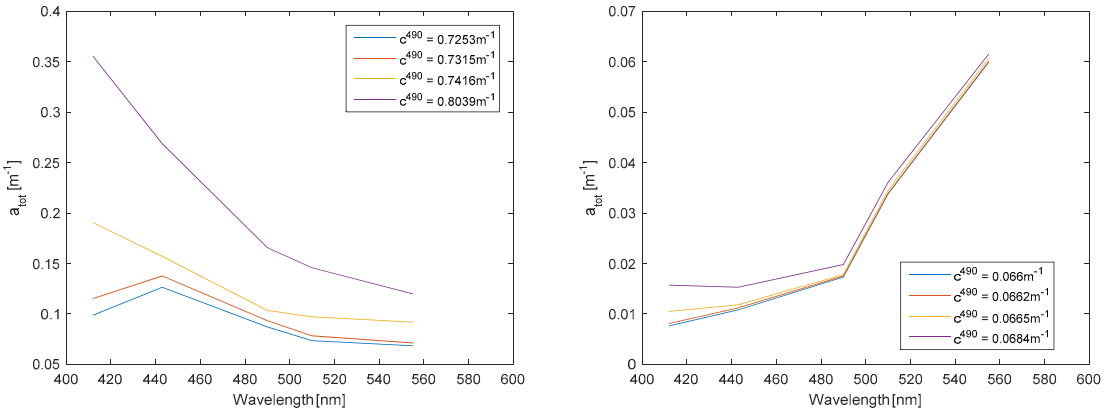

Figure 7. Plots of the total absorption coefficient (a_{tot}) for a set of Case 2 waters, [Chl] ~1.8 mg m^{-3}, (left panel) and a set of Case 1 waters, ([Chl] ~0.06 mg m^{-3} (right panel). Different curves correspond to varying total attenuation coefficients at 490 nm (c^{490}).

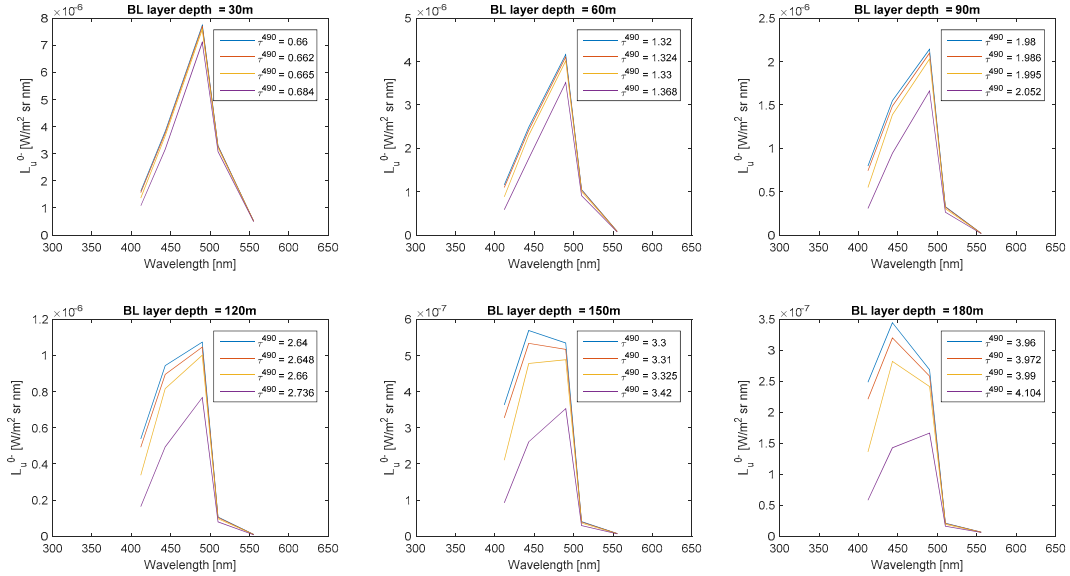

Figure 8. Upwelling radiance at surface for depths of a bioluminescent layer down to a depth of 180 m for very clear Case 1 water with [Chl] ~0.06 mg m^{-3}. The different curves of upwelling radiances correspond to different optical depths (τ^{490}), which are related to the varying concentrations of NAP and CDOM (linked to R_{NAP} and R_{CDOM}, respectively; see Figure 7). The intensity of the upwelling radiance is highest at 490 nm when the bioluminescent layer is shallow, but the maximum progressively blue-shifts as the layer is stimulated at greater depths.

A method to quantify the spectral shift of the surface upwelling radiance peak is to consider the ratio of radiances at two wavelengths. The ratio L_u^{490}/L_u^{443} decreases monotonically with optical depth at the BL layer for [Chl] ~0.06 mg m^{-3}. For [Chl] ~1.8 mg m^{-3} instead, the behavior becomes more complex and the ratio L_u^{490}/L_u^{510} first decreases then slightly increases and reaches an asymptotic value, dependent on the specific IOPs of the water column (Figure 9). The approach of the ratio L_u^{490}/L_u^{510} to an asymptotic value for [Chl] ~1.8 mg m^{-3} suggests that the same could happen for [Chl] ~0.06 mg m^{-3}, if the output radiances were to be computed at larger depths (i.e. larger optical depths). Simulated extended depth ranges and simulated hyperspectral radiances are planned to be part of a future study.

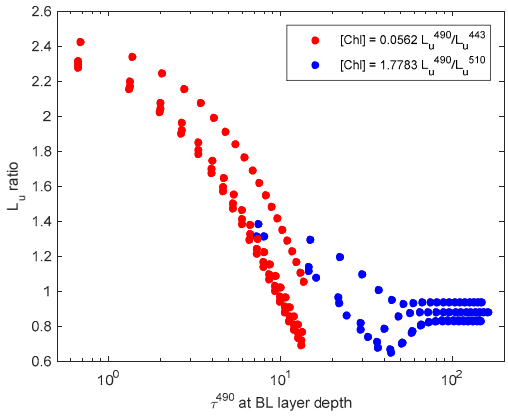

Figure 9. Ratios of surface upwelling radiances vs. optical depth at 490 nm (τ^{490}) for the set of Case 2 waters from Figs. 6 and 7(right panel), [Chl] ~1.8 mg m^{-3} (blue dots) and the set of Case 1 waters from Figs. 8 and 7(left panel), ([Chl] ~0.06 mg m^{-3} (red dots).

3. CONCLUSIONS

The data presented in this study highlights the importance of simultaneous consideration of bioluminescent signal and IOPs. The detectability of stimulated BL depends on the SNR of a radiometer (or of any other detector) and on the depth of the bioluminescent layer. High variability in IOPs and depth of the bioluminescent layer require extensive evaluation of the possible scenarios with interest in detecting and predicting the advantages and disadvantages of BL events and might be a useful tool to assess the vertical structure and ecology of bioluminescent organisms in the ocean.

4. ACKNOWLEDGEMENTS

This work was supported by the NOAA OER funded CIOERT (Cooperative Institute for Ocean Exploration, Research and Technology) - Novel Technology to Explore the Mesopelagic Ocean.

REFERENCES

[1] Herring P.J. and Widder E.A., [Bioluminescence], Academic Press, San Diego, 308-317 (2001).
[2] Wilson, T. and Hastings, J.W., "Bioluminescence," Annual Review of Cellular and Developmental Biology, 14, 197-230 (1998).
[3] Hastings, J.W., "Chemistries and colors of bioluminescent reactions: a review," Gene, 173, 5-11 (1996).
[4] Herring, P.J., "The spectral characteristics of luminous marine organisms," Proc. R. Soc. Lond. B 220, 183-217 (1983).
[5] Latz, M.I. and Rohr, J., "Glowing with the flow: ecology and applications of flow stimulated bioluminescence," Optics & Photonics News Oct. 16(10), 40-45 (2005).
[6] Mobley, C.D., [Light and Water: Radiative Transfer in Natural Waters], Academic Press (1994).
[7] Lapota, D., Galt, C., Losee, J., Huddell, H.D., Orzech, J.K. and Nealson, K.H., "Observations and measurements of planktonic bioluminescence in and around a milky sea," J. Exp. Mar. Biol. Ecol., 119, 55-81 (1988).
[8] Moline, M.A., Oliver, M.J., Mobley, C.D., Sundman, L., Bensky, T., Bergmann, T., Bissett, W.P., Case, J., Raymond, E. H. and Schofield, O.M.E., "Bioluminescence in a complex coastal environment: 1. Temporal dynamics of nighttime water-leaving radiance," J. Geophys. Res., 112, C11016 (2007).
[9] Twardowski, M.S., Claustre, H., Freeman, S.A., Stramski, D. and Huot, Y., "Optical backscattering properties of the "clearest" natural waters," Biogeosciences, 4, 1041-1058 (2007).
[10] Cramer C., Lykke K., Woodward, J. and Smith A., "Precise Measurement of Lunar Spectral Irradiance at Visible Wavelengths," Journal of Research of the National Institute of Standards and Technology, 118, 396-402 (2013).
[11] Rohr, J., Schoonmaker, J., Losee, J., Latz, M.I. and Hyman, M., "Flow visualization in the ocean-implications of laboratory bioluminescence experiments," Proc. Oceans, 1, 145 (1999).

[12] Widder, E.A. and Johnsen, S., "3D spatial point patterns of bioluminescent plankton: a map of the 'minefield'," Journal of Plankton Research, 22(3), 409-420 (2000).
[13] Oliver M. J., Moline, M.A., Mobley, C.D., Sundman, L. and Schofield, O.M.E., "Bioluminescence in a complex coastal environment: 2. Prediction of bioluminescent source depth from spectral water-leaving radiance," J. of Geophys. Research, 112 (2007).
[14] Pope, R.M. and Fry, E.S., "Absorption spectrum (380-700 nm) of pure water. II. Integrating cavity measurements," Appl. Opt. 36, 8710-8723 (1997).
[15] Ciotti, A.M., Lewis, M.R. and Cullen, J.J., "Assessment of the relationships between dominant cell size in natural phytoplankton communities and the spectral shape of the absorption coefficient," Limnol. Oceanogr., 47, 404-417 (2002).
[16] Roesler, C.S. and Perry, M.J., "In situ phytoplankton absorption, fluorescence emission, and particulate backscattering spectra determined from reflectance," J. Geophys. Res., 100(13), 279-13,294 (1995).
[17] Twardowski, M.S., Boss, E., Sullivan, J.M. and Donaghay, P.L., "Modeling the spectral shape of absorbing chromophoric dissolved organic matter. Mar. Chem., 89, 69-88 (2004).
[18] Loisel, H. and Morel, A., "Light scattering and chlorophyll concentration in case 1 waters: A reexamination," Limnol. Oceanogr., 43, 847-858 (1998).
[19] Morel, A., "Are the empirical relationships describing the bio-optical properties of case 1 waters consistent and internally compatible?," Journal of Geophysical Research, 114, C01016, (2009).
[20] Twardowski, M.S., Boss, E., Macdonald, J.B., Pegau, W.S., Barnard, A.H. and Zaneveld, J.R.V., "A model for estimating bulk refractive index from the optical backscattering ratio and the implications for understanding particle composition in Case I and Case II waters," Journal of Geophysical Research, 106(C7), 14,129-14,142 (2001).